MDPI

Article

Geochemistry of Mudstones/Silty Mudstones from the Qigequan Formation and Shizigou Formation in Yuejin-II Area, Southwestern Area of the Qaidam Basin: Implications for Sedimentary Environment and Sandstone-Type Uranium Mineralization

Cong Ao [1,2], Xue-Ming Teng [1,2,*], Xue-Bin Wei [3], Tao Lei [3], Duo Wang [3] and Jun Yang [1,2]

[1] Tianjin Center, China Geological Survey, Tianjin 300170, China; a_o_cong@163.com (C.A.); yangjun1249@126.com (J.Y.)
[2] Key Laboratory of Uranium Geology, China Geological Survey, Tianjin 300170, China
[3] China Petroleum Qinghai Oilfield Branch Exploration and Development Institute, China National Petroleum Corporation, Dunhuang 736202, China; wxbqhyjy@petrochina.com.cn (X.-B.W.); leitaoqh@petrochina.com.cn (T.L.); wangduoqh@petrochina.com.cn (D.W.)
* Correspondence: cugbtxm@126.com

Abstract: The Qaidam Basin has been the focus of sandstone-type uranium prospecting since the 1950s. In recent years, relying on the uranium geological survey project supported by the China Geological Survey, and the cooperation with the Qinhai oil company, drilling work at the Yuejin-II area in this basin has achieved breakthroughs on industrial-level sandstone-type uranium exploration. In this study, we present major, trace and REE geochemical analysis of the Qigequan Formation and the Shizigou Formation mudstones/silty mudstones collected from an industrial uranium ore drillholes in the Yuejin-II area. The Shizigou and Qigequan Formations exhibit signatures of non-intense alteration, low rock maturity and proximal provenance. The overall arid paleoclimatic conditions controlled the sedimentation of large volume of uranium rich materials. The period of relative humidity prompted the sedimentation of reduced agents. Aided by the neotectonic-induced slopes and tectonic windows, oxygenated fluids migrated along permeable layers and extracted the hexavalent uranium, transported in the form of uranyl ion (UO_2^{2+}). When the oxygen–uranium-rich fluids finally infiltrated into the reductive sand body, the hexavalent uranium was reduced to tetravalent uranium and deposited in the form of uranium compounds. Large-scale and centrally distributed reductive sand bodies provided favorable ore storage space for the sandstone-type uranium mineralization in the Yuejin-II area.

Keywords: mudstones/silty mudstones; provenance; paleoclimate; sandstone-type uranium mineralization; Yuejin-II area

1. Introduction

As the largest high-altitude terrestrial multi-energy intermontane basin in the northeastern Tibetan Plateau (Figure 1a), the Qaidam Basin preserves exceptionally thick Mesozoic and Cenozoic sediments of 3–16 km [1–11]. These sedimentary successions host many important clues to the process of northward expansion and exhumation of the Tibetan Plateau [2,12–19], and the climatic and environmental evolution of the Qaidam Basin and its adjacent regions, especially the aridification process of Central Asia [20–31].
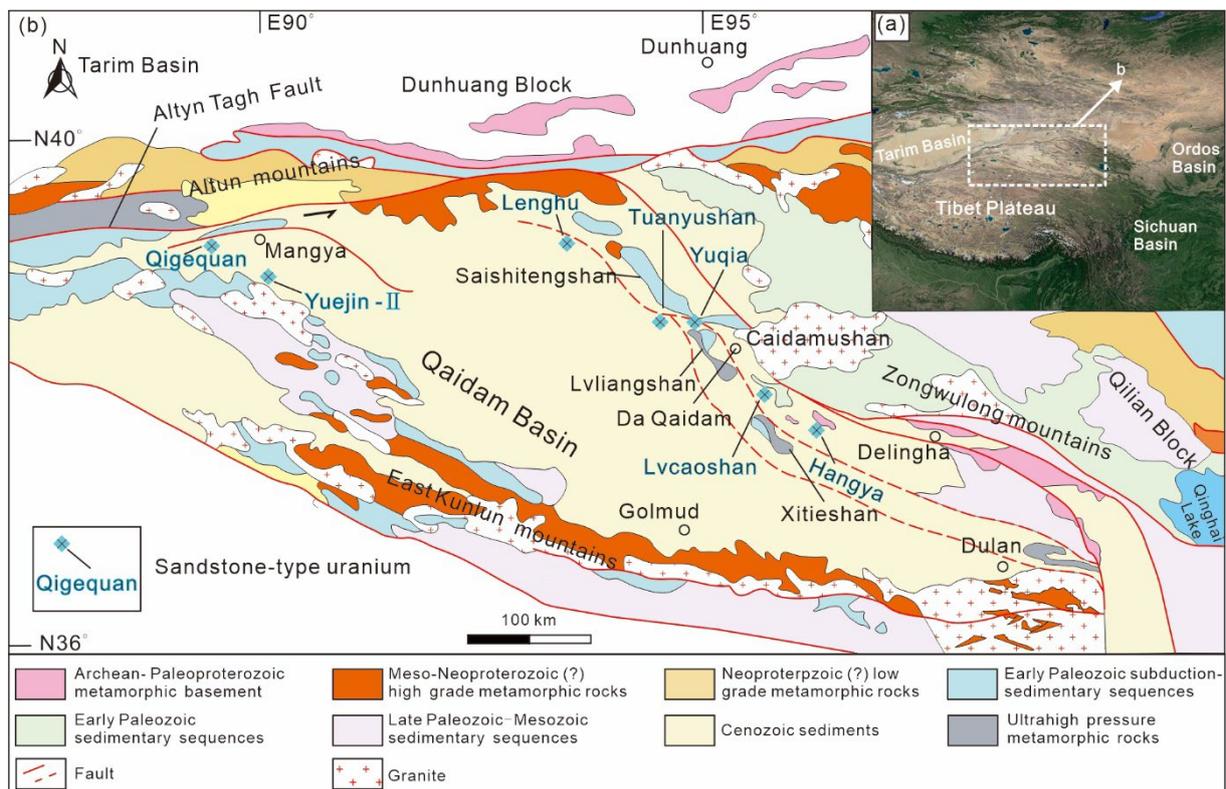
Figure 1. (**a**) Satellite map showing the location of the Qaidam Basin and (**b**) geological sketch map of the Altun-Qilian-Kunlun (AQK) orogenic system in the northern Tibet (modified after [32,33]).

Most previous climatic studies of the Tibet Plateau focused on the stable isotopes of carbonate rocks [27,29,30] and pollen composition of sediments [34–37], and they argued that the Late Cenozoic aridification affected by rapid and significant uplift of the Tibet Plateau and the land–sea redistribution associated with the continental collision of India and Eurasia [20,23,27]. The tectonic process of the Tibet Plateau and the subsequent climatic variations not only control sedimentary materials, but also the concentration and preservation of sedimentary-related energy resources, including oil and natural gas [38–40], coal [41–43] and sandstone-type uranium resources [44–48]. In particular, as the primary hydrocarbon source rocks, the mudstones/silty mudstones not only record important information on the paleoclimatic conditions [9], but also play one a significant part of source–reservoir–seal association for oil [49,50], source agent for coal [51,52], and serving as water-resisting layer or ore carrier for sandstone-type uranium deposits [53–55].

Factors that control the formation of exogenous uranium deposits are diverse and complicated, including the geological conditions, fluid type and behavior, reducing agents, etc. [56–60]. As early as 1983, Jiang [61] proposed that the paleoclimatic conditions play a basic but important role in controlling the above mentioned factors in all metallogenic stages of exogenous uranium deposits. It not only dominated the formation of ore-bearing rocks, but also tightly controlled the leaching, migration and precipitation of uranium [58,62–64]. However, only a few reports are available on the relationships between paleoclimate and sandstone-type uranium mineralization. Since 2000, with the deepening of prospecting for sandstone-type uranium deposits in the northern inland basin, the control of paleoclimate on the sandstone-type uranium mineralization has attracted the attention of more and more scholars [62,65–67]. Two aspects can be concluded regarding to the paleoclimate constraints on sandstone-type uranium mineralization. One is that the paleoclimate controls the formation of favorable ore-bearing strata, which not only restricts the structure and scale of sand body development of uranium reservoir, but also more importantly controls the types and spatial distribution of reduction agents inside and outside uranium reservoir during

the diagenetic stage. The second is that during the metallogenic period, the paleoclimate controlled the formation and properties of uranium-bearing oxidizing fluid. The hot and arid climate made it difficult for uranium to migrate, and it precipitated quickly and accumulated in certain parts.

With several decades of exploration investment in the Qaidam Basin, potential sandstone-hosted uranium rich prospecting area and spots have been gradually detected. In the last ten years especially, breakthroughs on industrial-level sandstone-type uranium exploration have been achieved in Yuejin-II area and Qigequan area, southwestern area of the Qaidam, with high grade, thick uranium bodies having been detected. The outstanding findings hint at great potential in sandstone-type prospecting and exploitation. In order to gain a preliminary understanding of the metallogenic mechanism of the sandstone-type uranium deposits in southwestern area of the Qaidam Basin, geochemical analyses on mudstones/silty mudstones collected from the Qigequan Formation and the Shizigou Formation in the Yuejin-II area has been performed in this study. Based on the results, this contribution aims to discuss the sedimentary environment and the paleoclimatic evolution and further to argue their constraints on sandstone-type uranium mineralization.

2. Geological Background

The Qaidam Basin, with an elevation of 2.7–3 km, covers an area of ca. 12×10^4 km^2. It is bounded by the Qilian Mountains to the north and east, East Kunlun Mountains to the south and Altun Mountains to the northwest [9,68] (Figure 1b). Since the 1950s, exploration work regarding sandstone-type uranium mineralization has been carried out. From the 1950s to the mid-1980s, several potential sandstone-hosted uranium rich spots (Lvcaosshan, Beidatan, Wucaishan, etc.) were discovered, which provided the basic clues to further prospecting. From the mid-1980s to 2000, more investigations and research projects followed in northern and eastern Qaidam Basin, including uranium hydrologic survey, airborne gamma-ray spectrometry measurement, and research on metallogenic condition and metallogenic prediction, which revealed high sandstone-type uranium potential in the Lenghu, Mahai, Wudaoliang and West Tuosu Lake areas. In the perspective of paleoclimate, hydrogeology, lithofacies paleogeography and uranium source, possible uranium-bearing strata of Lower and Middle Jurassic and Eocene Shizigou Formation and Quatenary Qigequan Formation have been reached a consensus. Since the 21st century, with more drilling work being carried out, more uranium prospecting target areas (Hangya, Yuxia, Tuanyushan, etc.) and layers (Eocene Xiaganchaigou Formation and Neogene Shang Ganchaigou Formation) have been verified. In particular, the investigations carried out on the southwestern Qaidam Basin revealed the prospective areas of Huatugou-Yingxiaongling area and the Former Mangya-Dong Chaishan area. In recent years, relying on the uranium geological survey project supported by the China Geological Survey, and the cooperation with the Qinhai oil company, drilling work at the Yuejin-II area and Qigequan area have achieved breakthroughs on industrial-level sandstone-type uranium exploration.

The Yuejin-II area is located at the southwestern area of the Qaidam Basin. This region is bounded by the Altun Mountains, Qiman Tagh Mountains and the inner basin Yingxiong Ridge Structural Belt with an area of ca. 2000 km^2. Most areas of Southwestern Qaidam Basin are covered by Quaternary sediments, and Paleogene and Neogene strata are only sporadically exposed at Yingxiong Rigde Structural Belt and similar structurally high part (Figure 2a). Among these, the Yuejin-II area has been well known for its high oil production since the mid-1980s. This oilfield is controlled by the Yuejin-II structure, which is located on the hanging wall of Alaer Fault and belonging to a third-order structure in the secondary Tiemulike anticline (Figure 2b). Based on seismic data, well-log information and paleontological analytic results, the basement in the study area is mainly composed by grayish-white, brownish-gray granite, unconformably overlain by Paleocene-Eocene Lulehe Formation, and further upwards, including strata of Oligocene Xia Ganchaigou Formation, Miocene Shang Ganchaigou Formation, Pliocene Xia Youshashan Formation, Shang Youshashan Formation and Shizigou Formation, and Pleistocene Qigequan Formation.

The Lulehe Formation is dominantly composed of greyish-white and brown conglomerate, intercalated with a small amount of brownish-red and tan mudstone. All the other Paleocene-Eocene strata consecutively exhibit conformable contact. The Xia Ganchaigou Formation is featured by two distinct members. The Lower Member is mainly composed of brownish-red, brown mudstone and sandy mudstone formed in oxidation environment, intercalated with brownish-yellow, brown siltstone, fine sandstone, gravelly sandstone and gravelly sandstone, while the Upper Member is represented by grey and dark grey mudstone, intercalated with grayish-white and brownish-yellow marl, grayish-white and brownish-yellow siltstone, fine sandstone, and a small amount of intra-clast carbonate rocks. The Shang Ganchaigou Formation is generally divided into two parts. The lower part is mainly composed of gray, dark gray mudstone and calcareous mudstone, intercalated with brownish-yellow, brown siltstone, fine sandstone, brownish-yellow intraclastic limestone and gray-white marlstone. The upper counterpart is dominated by brownish-red mudstone, intercalated with siltstone and gravelly sandstone. The Xia Youshashan Formation is characterized by the occurrence of brownish-red, tan and brownish-yellow mudstone and sandy mudstone, with a small amount of brownish-yellow, brownish-gray sandstone, gravelly sandstone and conglomerate. The Shang Youshashan Formation is comprised of light brown-red and brownish-yellow sandy mudstone, mudstone, brown-gray sandstone and gravelly sandstone, which are frequently intercalated with gray mudstone, calcareous mudstone and conglomerate. The Shizigou Formation is mainly composed by yellowish, light brownish-gray and light gray sandy mudstone, intercalated with gray, brownish-gray and brownish-yellow sandy conglomerate, occasionally with black carbonaceous mudstone in the middle part. The Quaternary Qigequan Formation is unconformably covering the Shizigou Formation. The lithologies of Qigequan Formation are composed of upper white halite and lower dominant gray conglomerate and gravel sandstone, with light gray, grayish-yellow mudstone and sandy mudstone (Figure 3).
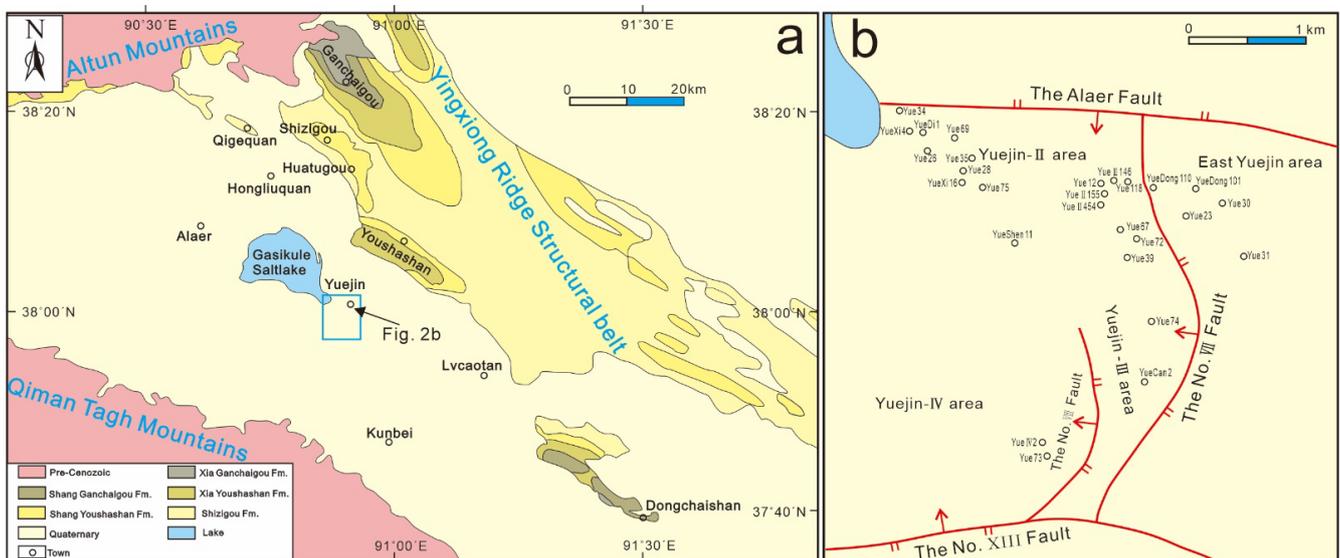

Figure 2. (**a**) Regional geological sketch of southwestern area of the Qaidam Basin and its adjacent orogenic areas (modified after [69]) and (**b**) schematic geological map of the Yuejin area to the main controlled faults and representative oilfield holes (modified after [70]).

Figure 3. Cenozoic stratigraphical framework and seismic reflectors of the southwestern area of the Qaidam Basin (modified after [69,71,72]). Detailed regional tectonic events see [9].

3. Characteristics of the Sandstone-Type Uranium Mineralization

Based on six boreholes drilled in the Yuejin-II area, three groups of uranium ore horizons have been detected (Figure 4).

The No. I group of uranium horizon is situated in the Qigequan Formation at the depth of 40–60 m. The ore-hosted rocks are dominantly composed of greenish-gray siltstone and fine sandstone. The No. II group of uranium horizon is at depth of 220–270 m, located around the unconformity between the Qigequan Formation and Shizigou Formation. This uranium horizon is the thickest ore-bearing layer with thickness varying from 6.2 m to 10.5 m. The ore-hosted rocks are composed by greenish-gray fine sandstone and pebbly sandstone. The 300–410-meter-deep No. III group of uranium horizon is composed of several longitudinal discontinuous ore-bearing strata with thickness in the range of 1.7–5.3 m. The ore-carried rocks of this horizon are greenish-gray fine sandstone and siltstone.

The ZKII-05 is one of the industrial uranium ore drillholes revealing the strata including Quaternary chemical accumulation of salt lake (0–41.68 m), the Qigequan Formation (41.68–268.11 m), the Shizigou Formation (268.11–465 m). The Qigequan Formation exhibits several distinct red rock series (including yellow-brown-red continental clastic rock associations) and black rock series (including green-gray-black continental clastic rock associations and coal-oil bearing rocks). Generally, the upper part is characterized by red rock series with only several relatively thin seams of black rock series, while the lower part is featured by black rock series. Comparatively, the Shizigou Formation is composed of overall greenish rocks with plenty of red rock layers. Both the uranium anomaly, uranium mineralized layer and uranium industrial layers occur at transition of red and black rock series (Figure 5). The most favorable sedimentary facies for uranium bearing sequences are dominantly by braided-meandering river and braided-meandering river delta facies, subsequently by alluvial fan, alluvial fan delta, shore-shallow lacustrine facies [73–76]. Abudukeyumu et al. [77] reported that disseminated uranyl silicates (coffinite) and uraninite are the main uranium minerals situated in the ore-bearing strata.

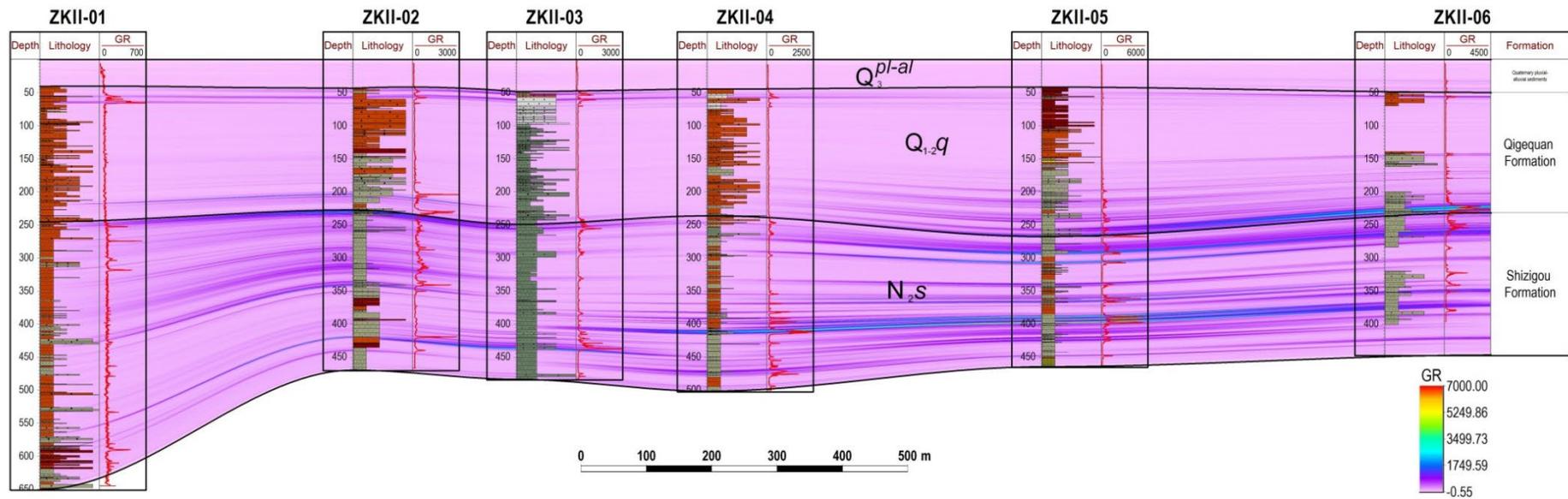**Figure 4.** The well-tie profile to illustrate uranium ore horizons among industrial sandstone-hosted uranium boreholes in the Yuejin-II area (the contour-filled color was based on the Natural Gamma Logging Values (GR), with high values representing the uranium horizons). Q_3^{pl-al}-Quaternary pluvial-alluvial sediments, $Q_{1-2}q$-Quaternary Qigequan Formation, N_2s-Neogene Shizigou Formation.
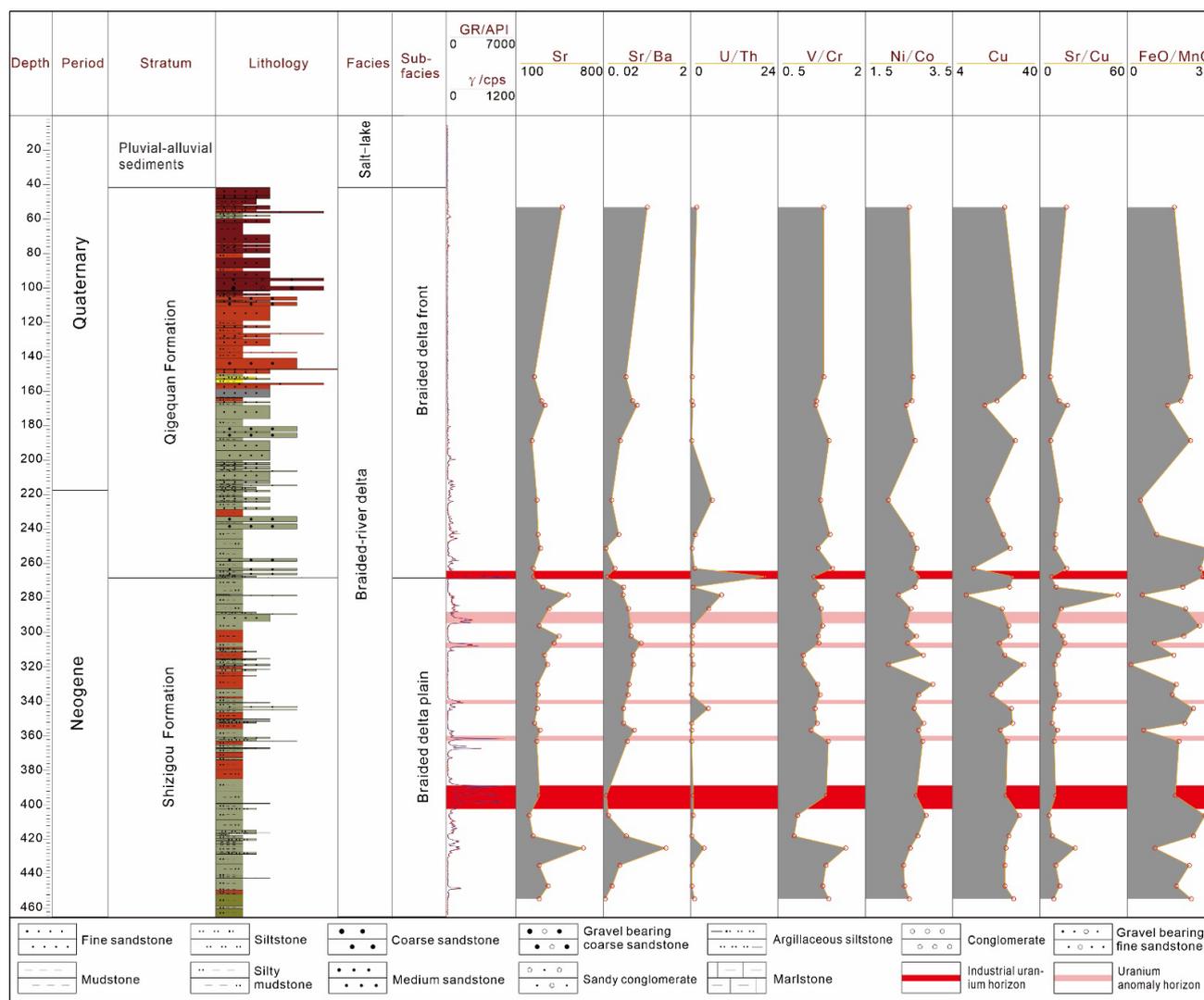
Figure 5. The comprehensive columns of ZKII-05 to illustrate the strata, lithologies, facies, sub-facies and variation trend of representative elements and elemental ratios. The filled color of the lithology column represents its respective catalog color.

4. Sampling and Analytical Methods

Samples for this study are all from ZKII-05. In total, 31 mudstones/siltstone samples belonging to the Qigequan Formation and the Shizigou Formation were collected at different depths from 45 m to 454.5 m. For a comparative study, three associated fine-grained sandstones from Qigequan Formation were also collected.

All these samples were crushed and powdered to 200 mills for whole rock geochemical analyses. The whole rock geochemical analyses were conducted at the laboratory of Tianjin Center, China Geological Survey. The major elements were determined by X-ray fluorescence (XRF), with analytical uncertainties ranging from 1 to 2%. Loss on ignition was obtained using about 1 g of sample powder heated at 980 °C for 30 min. The trace elements (including REEs) were determined as solute by XSERIES-II inductively coupled plasma mass spectrometry (ICP-MS). About 50 mg of powder was dissolved for about 7 days at ca. 100 °C using HF–HNO$_3$ (10:1) mixtures in screw-top Teflon beakers, followed by evaporation to dryness. The material was dissolved in 7N HNO$_3$ and taken to incipient dryness again, and then was re-dissolved in 2% HNO$_3$ to a sample/solution weight ratio of 1:1000. The analytical errors vary in the range of >5% depending on the concentration of any given element.

5. Results and Discussions

Whole rock geochemical data, including major, trace and rare earth elements for rock samples from the Qigequan Formation and Shizigou Formation, ZKII-05 are presented in Supplementary Material Table S1. The Si, Al, Ca, Na and K contents, REEs and other selected trace elements for all the samples were normalized to the Upper Continental Crust (UCC, ref. [78]) as shown in Figure 6.
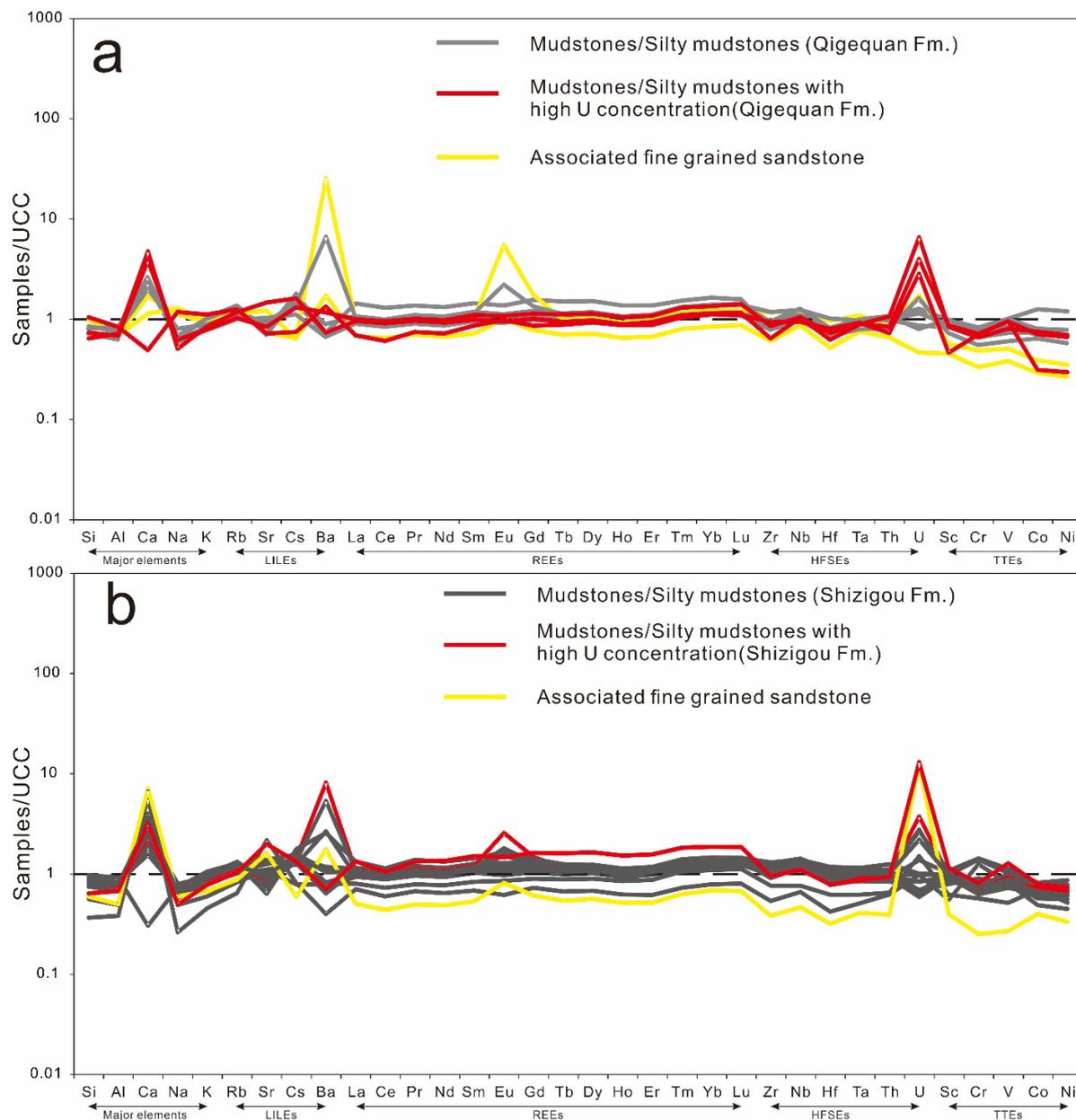

Figure 6. Upper continental crust-normalized variation diagrams for rocks samples from Qigequan Formation (**a**) and Shizigou Formation (**b**) in this study. Upper continental crust values are from [78].

5.1. Evaluation on Factors That Control the Final Chemical Components during Diagenetic Process

Generally, during the diagenetic process, factors that control the final chemical components of siliciclastic sedimentary rocks include (1) grain-size effect due to hydrodynamic sorting [9,79], (2) chemical weathering throughout the sedimentary process and outcrop stage [80,81], and (3) burial diagenetic K-metasomatism and later metamorphism [82,83]. In order to utilize geochemical data to deduce the signature of source rock or tectonic setting, influences on the above three factors for the samples in this study must be evaluated.

During the process of hydrodynamic sorting, relatively coarse-grained sediments which contain more quartz and feldspar are likely to display a low Al/Si ratio, while relatively fine-grained sediments usually exhibit high Al/Si rations due to high contents of phylo-silicates and clay minerals [9]. In the UCC-normalized spider diagram (Figure 6a), the three associated fine-grained sandstones display relatively low REE and other element abundances (e.g., Th, Zr and Hf), and high Ba and Eu abundance. The relatively high $\sum$REE in mudstones can be attributed to enrichment of clays, while sandstones with high Ba abundances and positive Eu/Eu* values due to elemental concentration by high content of plagioclase. Those mudstone/silty mudstone samples (as shown in red color in Figure 6) with high U contents indicate the occurrence with absorbed U or uranium minerals. The overall similar UCC-normalized patterns of mudstones and three associated fine-grained sandstones suggest that they were likely derived from the same UCC-sourced region. The chemical differentiation between mudstones and the associated sandstones can be attributed to the effect of physical sorting rather than different source rocks. In that case, compared to sandstone, conglomerate and other large grain sized and poorly sorted sedimentary rocks, mudstone/silty mudstone could be more efficiency to deduce the provenance, paleoclimate and tectonic setting due to its relatively homogeneous composition [9,84,85].

In terms of the influence of chemical weathering, the major elements-based chemical index of alteration (CIA = $Al_2O_{3mol}/(Al_2O_{3mol} + CaO^*_{mol} + Na_2O_{mol} + K_2O_{mol}) \times 100\%$ in molecular proportions [80,86]) has been widely used to evaluate the degree of chemical weathering relative to source and to reconstruct the paleo-weathering conditions of ancient mudstones [9,82,84,85]. In particular, the CaO^*_{mol} represents Cao_{mol} solely from the silicate fraction. However, due to the existing chemical-related CaO, the CaO_{mol} in silicates could be first empirically calculated by the formula of $CaO^{em}_{mol} = CaO_{mol} - (10/3 \times P_2O_{5mol})$, then if the $CaO^{em}_{mol} \leq Na_2O_{mol}$, we accepted the value of CaO^{em}_{mol} as the CaO^*_{mol}. Otherwise, we assumed that the real moles of silicate $CaO^*_{mol} = Na_2O_{mol}$ [86]. However, for the Cenozoic mudstones, the diagenetic K-metasomatism may significantly change the bulk composition and results in the enrichment of K that affected the CIA values [9,82]. In order to eliminate the influence of diagenetic K-metasomatism on CIA value, a ternary diagram of $Al_2O_3 - (CaO^* + Na_2O) - K_2O$ (A-CN-K ternary diagram) proposed by Nesbitt and Young [87] can be adopted. In the A-CN-K ternary diagram (Figure 7), solid line (line 1) represents the best-fit straight line through these mudstones, and its intersection with the Pl-Kfs join indicating the composition of the un-weathered source rock which possibly derived from the UCC, while the dash lines with arrows (line 2) representing predicted weathering trends of un-weathered UCC rocks without the enrichment of K. It extends upwards parallel to the A-CN until it intersects with the A-K join, then follows the A-K join until to the A apex. In addition, a K-corrected CIA ($CIA_{corrected} = Al_2O_{3mol}/(Al_2O_{3mol} + CaO^*_{mol} + Na_2O_{mol}) \times (100 - 11.5)$ can be accepted to evaluate the chemical weathering excluding the K-metasomatism. The value of 11.5 represents the molecular percent of K_2O of the un-weathered source rocks as plotted in Figure 7. All the $CIA_{corrected}$ values for these rock samples are in the range of 48.19–63.69 (Table S1). The values below the worldwide average shale CIA values of ca. 70–75 indicate fresh or slightly chemical weathered process, which could exhibit weak effect on the variations of these rocks during the diagenetic process [88].

In summary, the mudstones samples collected in this study can be utilized to deduce the signature of source rock or tectonic setting.
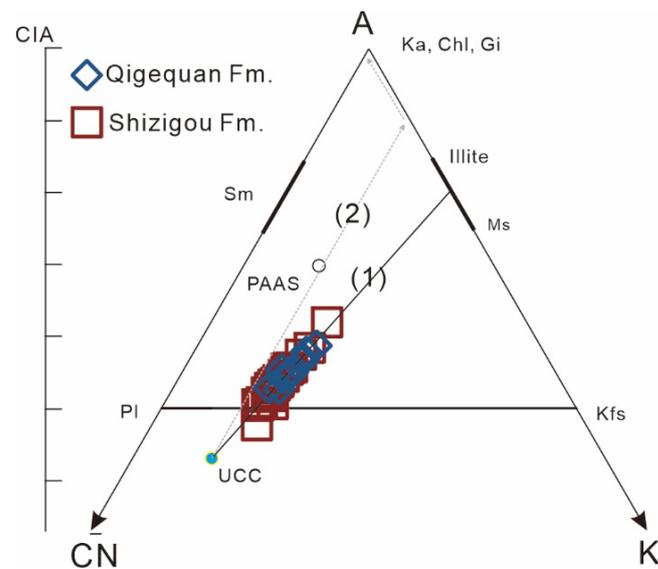
Figure 7. A–CN–K ternary diagrams for rock samples in this study. Abbreviations: Ka—kaolinite; Chl—chlorite; Gi—Gibbsite; Sm—smectite; Mu-muscovite; Pl—plagioclase; Kfs—K-feldspar.

5.2. Sedimentary Provenance

As discussed above, these mudstones exhibit a signature of UCC-derived source origin through the UCC-normalized elemental patterns (Figure 6). Though all the mudstones exhibit variable SiO_2 content and Al_2O_3 content, the Al_2O_3/SiO_2 ratios are varying from 0.19–0.26, indicating signatures of non-intense alteration, low rock maturity and proximal provenance [89,90]. In addition, various major and trace element provenance diagrams for clastic sediments have been erected by previous studies. The La/Th values of these mudstones varying in the range of 2.66–4.24, while the Hf content is in the range of 1.70–6.26 ppm. On the La/Th-Hf diagram (Figure 8a; [91]), the mudstone samples are dominantly plotted in the same area indicating a felsic source. Discriminated from the binary diagram of Th/Sc-Zr/Sc (Figure 8b; [92]), all the mudstones also exhibit uniform geochemical indices that, similarly to felsic, featured upper continental crust. In particular, the average Zr content for all the mudstone samples is 193.04 ppm, which is also close to that of the average upper continental crust [93], further indicating the felsic featured upper continental crust provenance without the recycling of old sediments.

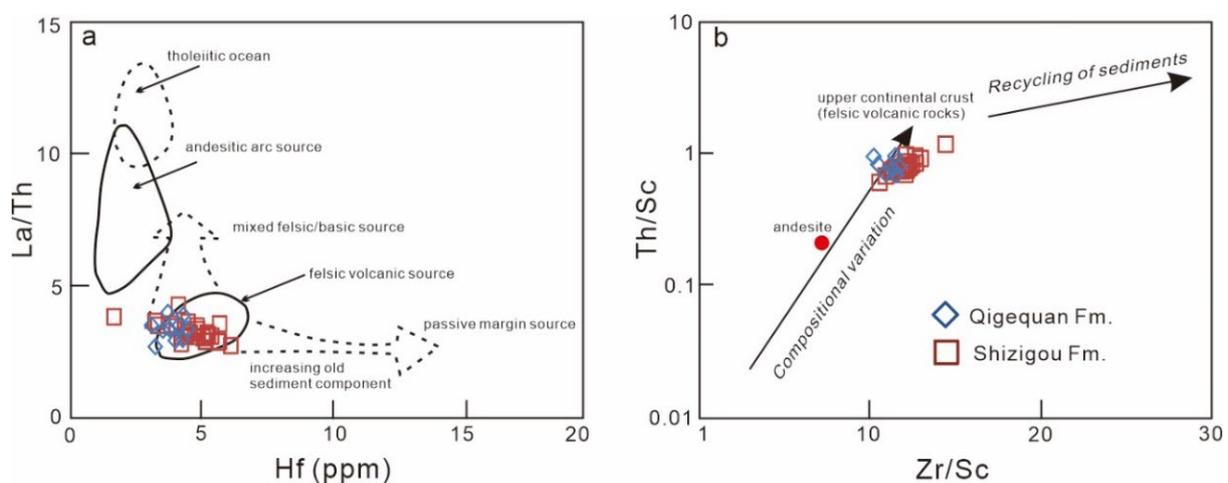**Figure 8.** Discrimination binary diagrams of La/Th vs. Hf (**a**) and Th/Sc vs. Zr/Sc (**b**) illustrating sedimentary provenance of the mudstones/silty mudstones collected from the Shizigou Formation and the Qigequan Formation in the Yuejin-II area.

5.3. Sedimentary Environment

5.3.1. Paleo-Salinity

Geochemical indicators to distinguish the paleo-salinity usually include the Sr, Ba contents and the Sr/Ba ratio [94,95]. The Sr/Ba value for sediments deposited in the fresh water is usually less than 1, while that deposited in the salted water usually greater than 1. The mudstones from the Qigequan Formation exhibit Sr/Ba value in the range of 0.40–1.02, while that of the mudstones from the Shizigou Formation vary within the range of 0.06–0.88, except one sample collected at 425 m with a value of 1.44 (Figure 5). The Sr/Ba value for all the rocks indicates the fresh water is crucial for the sedimentation, without the input of salty water.

5.3.2. Paleo-Redox Conditions

The redox conditions during sedimentation could affect the solubility and occurrence state of redox-sensitive trace elements. Thus, through signatures of these redox-sensitive trace elements in sediments, the redox conditions can be discussed [96–98]. The U, Mo, Cr, V and Co are easier to make soluble under oxidation conditions and insoluble under reduction conditions. In oxic settings, these elements usually exist as dissolved and migratable ion species of uranyl ion (UO_2^{2+}), molybdate ion (MoO_4^{2-}), chromate anion (CrO_4^{2-}), vanadate oxyanions (HVO_4^{2-} and $H2VO_4^{-}$) and Co^{2+}, respectively. In the oxygen poor environment, these elements tend to become authigenically enriched with almost no migration during diagenesis [97,99–103]. The Ni, Cu, Zn and Cd are generally precipitated under oxygen deficit conditions, while in the oxygen-rich environment, they are becoming more soluble. Several parameters to discriminate the redox conditions of the water during the sedimentation have been established by Jones and Manning [104], including U/Th, V/Cr and Ni/Co values. Except for the absorbed U-rich mudstones, the other mudstones from the Qigequan or Shizigou Formation exhibit relatively narrow variations of U/Th (<0.75) ratios indicating the overall oxygen-rich water during sedimentation. The V/Cr and Ni/Co values of these mudstones from the Qigequan Formation (V/Cr: 1.12–1.44, with average of 1.26, Ni/Co: 2.03–2.75, with average of 2.53) and the Shizigou Formation (V/Cr: 0.77–1.67, with average of 1.19, Ni/Co: 2.02–3.05, with average of 2.61) also indicate oxygen-rich water during sedimentation.

5.3.3. Paleoclimatic Conditions

As one of the methods of paleoclimate discrimination, element geochemistry, such as major/trace elements or ratios of Cu, Sr/Cu, Al_2O_3/MgO and FeO/MnO provide significant information. The Cu is mainly transported into sediments by organic matter, so it is often used as an ideal indicator to discuss organic matter flux [97]. The Sr/Cu ratio between 1.3 and 5.0 indicates a warm and humid climate, while the value greater than 5.0 indicates an arid climate [105]. The FeO/MnO ratio is also indicative of climate variations. The content of Mn is relatively high in arid environment and low in relatively humid conditions, while Fe is easy to precipitate rapidly with Fe(OH) colloid in humid environment. Therefore, the high value of FeO/MnO ratio in sediments corresponds to warm and humid climate, while the low value is the response of dry and hot climate [94]. All the Sr/Cu values for these rocks are greater than 5, indicating the overall arid climate. In general, the high Cu contents indicate more organic carbon, representing relatively humid and reductive conditions. As shown in Figure 5, the industrial uranium (red filled bars) and uranium anomaly horizons (pink filled bars) generally occur at the area of decrease in Cu content, indicating the redox boundaries. The industrial uranium horizons exhibit relatively extensive decrease in the Cu content when compared to the anomaly horizons. The corresponding variations of FeO/MnO ratios indicate alternated relatively dry and relatively humid climates (Figure 5).

5.4. Implications for Uranium Mineralization

The post-Neogene sediments in southwestern Qaidam Basin have not experienced strong alteration, exhibiting low maturity and proximal provenance signature, with dominantly braided delta front deposition and sand body development. On the whole, the paleoclimatic conditions during the depositional stage from the Shizigou Formation to the Qigequan Formation in the Yuejin-II area were arid, favorable for the sedimentation of large volume of uranium rich materials. However, there existed periods of relative humidity and relative drought in the overall drought situation. In the relative humid period, strata with reduced agents were deposited, while in the relative dry period, uranium-carried felsic rocks eroded and were transported to the inner basin, and deposited as part of oxidized strata. The uranium-containing oxidized strata laid the foundation for further sandstone-type uranium mineralization. Between the Oligocene and Quaternary, the Qaidam Basin underwent contraction, accompanied by the formation of series of NWW-SEE compressional anticlines [106,107]. The uplifted anticlines formed under the influence of neotectonic movement promoted development of the slopes and tectonic windows, which are crucial for the migration of oxygen-rich fluids [108,109]. The oxygen-rich fluids migrated along the permeable layers, and extracted the hexavalent uranium and transported in the form of uranyl ion (UO_2^{2+}). When the oxygen-uranium rich fluids infiltrated into the reductive sand body formed under braided river environment, these uranyl ions were reduced to tetravalent uranium and deposited in the form of uranium compounds. Large scale and centrally distributed reductive sand bodies provides favorable ore storage space for certain scale of sandstone-type uranium mineralization in the Yuejin-II area.

6. Conclusions

(1) The Shizigou Formation and Qigequan Formation exhibit signatures of non-intense alteration, low rock maturity and proximal provenance, with dominantly braided delta front deposition and sand body development.

(2) The overall arid paleoclimatic conditions controlled the sedimentation of large volume of uranium rich materials. The period of relative humidity prompted the sedimentation of reduced agents. The neotectonic-induced slopes and tectonic windows provided pathways for oxygen-rich fluids that infiltrated along permeable layers and extracted the hexavalent uranium and transported in the form of uranyl ion (UO_2^{2+}). When the oxygen-uranium rich fluids entered the reductive sand body, the hexavalent uranium was reduced to tetravalent uranium and deposited in the form of uranium compounds.

(3) Large scale and centrally distributed reductive sand bodies provided favorable ore storage space for certain scale of sandstone-type uranium mineralization in the Yuejin-II area.

References

1. Hanson, A.D.; Ritts, B.D.; Zinniker, D.; Moldowan, J.M.; Biffi, U. Upper Oligocene lacustrine source rocks and petroleum systems of the northern Qaidam basin, northwest China. *AAPG Bull.* **2001**, *85*, 601–619.
2. Tapponnier, P. Oblique stepwise rise and growth of the Tibet plateau. *Science* **2001**, *294*, 1671–1677. [CrossRef] [PubMed]
3. Rieser, A.B.; Neubauer, F.; Liu, Y.; Ge, X. Sandstone provenance of north-western sectors of the intracontinental Cenozoic Qaidam basin, western China: Tectonic vs. climatic control. *Sediment. Geol.* **2005**, *177*, 1–18. [CrossRef]
4. Yin, A.; Dang, Y.Q.; Zhang, M.; McRivette, M.W.; Burgess, W.P.; Chen, X.H. Cenozoic tectonic evolution of Qaidam basin and its surrounding regions (part 2): Wedge tectonics in southern Qaidam basin and the Eastern Kunlun Range. In *Whence the Mountains? Inquiries into the Evolution of Orogenic Systems: A Volume in Honor of Raymond A. Price*; Geological Society of America: Boulder, CO, USA, 2007; pp. 369–390.
5. Yin, A.; Manning, C.E.; Lovera, O.; Menold, C.A.; Chen, X.H.; Gehrels, G.E. Early Paleozoic tectonic and thermomechanical evolution of ultrahigh-pressure (UHP) metamorphic rocks in the northern Tibetan Plateau, northwest China. *Int. Geol. Rev.* **2007**, *49*, 681–716. [CrossRef]
6. Yin, A.; Dang, Y.Q.; Wang, L.C.; Jiang, W.M.; Zhou, S.P.; Chen, X.H.; Gehrels, G.E.; Mcrivette, M.W. Cenozoic tectonic evolution of Qaidam basin and its surrounding regions (Part 1): The southern Qilian Shan-Nan Shan thrust belt and northern Qaidam basin. *Geol. Soc. Am. Bull.* **2008**, *120*, 813–846. [CrossRef]
7. Yin, A.; Dang, Y.Q.; Zhang, M.; Chen, X.H.; McRivette, M.W. Cenozoic tectonic evolution of the Qaidam basin and its surrounding regions (Part 3): Structural geology, sedimentation, and regional tectonic reconstruction. *Geol. Soc. Am. Bull.* **2008**, *120*, 847–876. [CrossRef]
8. Wang, G.C.; Zhang, K.X.; Cao, K.; Wang, A.; Xu, Y.D.; Meng, Y.N. Expanding processes of the Qinghai-Tibet Plateau during Cenozoic: An insight from spatio-temporal difference of Uplift. *Earth Sci. J. China Univ. GeoSci.* **2010**, *35*, 713–727, (In Chinese with English Abstract).
9. Jian, X.; Guan, P.; Zhang, W.; Feng, F. Geochemistry of Mesozoic and Cenozoic sediments in the northern Qaidam basin, northeastern Tibetan Plateau: Implications for provenance and weathering. *Chem. Geol.* **2013**, *360–361*, 74–88. [CrossRef]
10. Yu, P.H.; Ma, J.L.; Liao, J.B.; Li, Z.Y.; Di, J. Geochemistry and paleoenvironment significance of Lulehe Formation/Xiaganchaigou Formation located in the north area of Qaidam Basin. *Arid Land Geogr.* **2020**, *43*, 679–686, (In Chinese with English Abstract).
11. Sang, S.P.; Lu, H.J.; Ye, J.C.; Pan, J.W.; Li, H.B. Sediment Recycling in the Northern Qaidam Basin Margin during the Cenozoic: A Case Study from the Dahonggou Section. *Geol. China* **2021**. Available online: https://kns.cnki.net/kcms/detail/11.1167.P.20210301.1338.002.html (accessed on 1 March 2021).
12. Harrison, T.M.; Copeland, P.; Kidd, W.S.F.; Yin, A. Raising tibet. *Science* **1992**, *255*, 1663–1670. [CrossRef]
13. Chung, S.L.; Lo, C.H.; Lee, T.Y.; Zhang, Y.; Xie, Y.; Li, X.; Wang, K.L.; Wang, P.L. Diachronous uplift of the Tibetan Plateau starting 40 myr ago. *Nature* **1998**, *394*, 769–773. [CrossRef]
14. Zheng, H.B.; McAulay Powell, C.; An, Z.S.; Zhou, J.; Dong, G.R. Pliocene uplift of the northern Tibetan Plateau. *Geology* **2000**, *28*, 715–718. [CrossRef]
15. Wang, C.; Zhao, X.; Liu, Z.; Lippert, P.C.; Graham, S.A.; Coe, R.S.; Yi, H.; Zhu, L.; Liu, S.; Li, Y. Constraints on the early uplift history of the Tibetan Plateau. *Proc. Natl. Acad. Sci. USA* **2008**, *105*, 4987–4992. [CrossRef] [PubMed]
16. Wang, G.C.; Cao, K.; Zhang, K.X.; Wang, A.; Liu, C.; Meng, Y.N.; Xu, Y.D. Spatio-temporal framework of tectonic uplift stages of the Tibetan Plateau in Cenozoic. *Sci. China Earth Sci.* **2011**, *54*, 29–44. [CrossRef]
17. Clark, M.K. Early Tibetan Plateau uplift history eludes. *Geology* **2011**, *39*, 991–992. [CrossRef]
18. Ge, J.; Ying, D.; Zhang, Z.; Zhao, D.; Li, O.; Yan, Z.; Liang, Y.; Wu, H.; Oldfield, F.; Guo, Z. Major changes in East Asian climate in the mid-Pliocene: Triggered by the uplift of the Tibetan Plateau or global cooling? *J. Asian Earth Sci.* **2013**, *69*, 48–59. [CrossRef]
19. Zhang, C.; Wang, S.B.; Yu, R.A.; Cheng, Y.H.; Feng, P.; Yu, H. Mesozoic-cenozoic tectonic evolution and uranium source analysis in northwestern Qaidam basin. *North China Geol.* **2021**, *44*, 67–73, (In Chinese with English Abstract).
20. Molnar, P.; England, P.; Joseph, M. Mantle dynamics, uplift of the Tibetan plateau and the Indian monsoon. *Rev. Geophys.* **1993**, *31*, 357–396. [CrossRef]
21. Ramstein, G.; Fluteau, F.; Besse, J.; Joussaume, S. Effect on orogeny, platemotion and land–sea distribution on Eurasian climate change over the past 30 million years. *Nature* **1997**, *386*, 788–795. [CrossRef]
22. Rea, D.K.; Snoeckx, H.; Joseph, L.H. Late Cenozoic eolian deposition in the North Pacific: Asian drying, Tibetan uplift, and cooling of the northern hemisphere. *Paleoceanography* **1998**, *13*, 215–224. [CrossRef]
23. An, Z.; Kutzbach, J.E.; Prell, W.L.; Porter, S.C. Evolution of Asian monsoons and phased uplift of the Himalaya Tibetan plateau since late Miocene times. *Nature* **2001**, *411*, 62–66.

24. Guo, Z.T.; Peng, S.Z.; Hao, Q.Z.; Biscaye, P.E.; An, Z.S.; Liu, T.S. Late Miocene–Pliocene development of Asian aridification as recorded in the Red-Earth Formation in northern China. *Glob. Planet. Chang.* **2004**, *41*, 135–145. [CrossRef]

25. Dupont-Nivet, G.; Krijgsman, W.; Langereis, C.G.; Abels, H.A.; Dai, S.; Fang, X. Tibetan plateau aridification linked to global cooling at the Eocene–Oligocene transition. *Nature* **2007**, *445*, 635–638. [CrossRef] [PubMed]

26. Katz, M.E.; Miller, K.G.; Wright, J.D.; Wade, B.S.; Browning, J.V.; Cramer, B.S.; Rosenthal, Y. Stepwise transition from the Eocene greenhouse to the Oligocene icehouse. *Nat. Geosci.* **2008**, *1*, 329–334. [CrossRef]

27. Kent-Corson, M.L.; Ritts, B.D.; Zhuang, G.; Bovet, P.M.; Graham, S.A.; Chamberlain, C.P. Stable isotopic constraints on the tectonic, topographic, and climatic evolution of the northern margin of the Tibetan Plateau. *Earth Planet. Sci. Lett.* **2009**, *282*, 158–166. [CrossRef]

28. Sun, J.; Ye, J.; Wu, W.; Ni, X.; Bi, S.; Zhang, Z.; Liu, W.; Meng, J. Late Oligocene-Miocene mid-latitude aridification andwind patterns in the Asian interior. *Geology* **2010**, *38*, 515–518. [CrossRef]

29. Zhuang, G.; Hourigan, J.K.; Koch, P.L.; Ritts, B.D.; Kent-Corson, M.L. Isotopic constraints on intensified aridity in Central Asia around 12 Ma. *Earth Planet. Sci. Lett.* **2011**, *312*, 152–163. [CrossRef]

30. Miao, Y.; Herrmann, M.; Wu, F.; Yan, X.; Yang, S. What controlled Mid–Late Miocene long-term aridification in Central Asia? Global cooling or Tibetan Plateau uplift: A review. *Earth Sci. Rev.* **2012**, *112*, 155–172. [CrossRef]

31. Jia, Y.X.; Wu, H.B.; Zhang, W.C.; Li, Q.; Yu, Y.Y.; Zhang, C.X.; Sun, A.Z. Quantitative cenozoic climatic reconstruction and its implications for aridification of the northeastern Tibetan Plateau. *Palaeogeogr. Palaeocl.* **2021**, *567*, 110244. [CrossRef]

32. Zhang, J.X.; Yu, S.Y.; Mattinson, C.G. Early Paleozoic polyphase metamorphism in northern Tibet, China. *Gondwana Res.* **2017**, *41*, 267–289. [CrossRef]

33. Ren, Y.F.; Chen, D.L.; Kelsey, D.E.; Gong, X.K.; Liu, L.; Zhu, X.H.; Yang, S.J. Metamorphic evolution of a newly identified Mesoproterozoic oceanic slice in the Yuka terrane and its implications for a multi-cyclic orogenic history of the North Qaidam UHPM belt. *J. Meta. Geol.* **2018**, *36*, 463–488. [CrossRef]

34. Wang, J.; Wang, Y.J.; Liu, Z.C.; Li, J.Q.; Xi, P. Cenozoic environmental evolution of the Qaidam Basin and its implications for the uplift of the Tibetan Plateau and the drying of central Asia. *Palaeogeogr. Palaeoclimatol. Palaeoecol.* **1999**, *152*, 37–47. [CrossRef]

35. Wang, Y.; Mosbrugger, V.; Zhang, H. Early to Middle Jurassic vegetation and climatic events in the Qaidam Basin, Northwest China. *Palaeogeogr. Palaeoclimatol. Palaeoecol.* **2005**, *224*, 200–216. [CrossRef]

36. Wang, X.; Qiu, Z.; Li, Q.; Wang, B.; Qiu, Z.; Downs, W.R.; Xie, G.; Xie, J.; Deng, T.; Takeuchi, G.T.; et al. Vertebrate paleontology, biostratigraphy, geochronology, and paleoenvironment of Qaidam Basin in northern Tibetan Plateau. *Palaeogeogr. Palaeoclimatol. Palaeoecol.* **2007**, *254*, 363–385. [CrossRef]

37. Miao, Y.; Fang, X.; Herrmann, M.; Wu, F.; Zhang, Y.; Liu, D. Miocene pollen record of KC-1 core in the Qaidam Basin, NE Tibetan Plateau and implications for evolution of the East Asian monsoon. *Palaeogeogr. Palaeoclimatol. Palaeoecol.* **2011**, *299*, 30–38. [CrossRef]

38. Ma, F.; Yang, W.; Zhang, Y.S.; Li, H.Z.; Xie, M.; Sun, X.J.; Wang, P.; Bai, Y.D. Characterization of the reservoir-caprock of the large basement reservoir in the Dongping field, Qaidam Basin, China. *Energy Explor. Exploit.* **2018**, *36*, 1498–1518. [CrossRef]

39. Li, J.; Zeng, L.; Li, W.; Zhang, Y.; Cai, Z. Controls of the Himalayan deformation on hydrocarbon accumulation in the western Qaidam Basin, northwest China. *J. Asian Earth Sci.* **2019**, *174*, 294–310. [CrossRef]

40. Chen, K.F.; Zhou, S.X.; Li, J.; Zhang, C.; Sun, Z.X.; Li, P.P.; Meng, B.K. Geochemical characteristics of natural gas and hydrocarbon charge history in the Western Qaidam Basin, Northwest China. *Geofluids* **2020**, *2020*, 2954758. [CrossRef]

41. Liu, T.; Wang, T.; Zhan, W. Analysis on structural control of coal distribution in the northern Qaidam Basin, NW China. *Acta Geol. Sin.* **2008**, *82*, 690–696, (In Chinese with English Abstract).

42. Zhan, W.F.; Lin, L.; Sun, H.B.; Sun, J.F. Tectonic evolution and structural control of coal in northern margin of Qaidam Basin coal-bearing zone. *Coal Geol. China* **2008**, *33*, 500–504, (In Chinese with English Abstract).

43. Lu, J.; Zhou, K.; Yang, M.F.; Shao, L.Y. Jurassic continental coal accumulation linked to changes in palaeoclimate and tectonics in a fault-depression superimposed basin, Qaidam Basin, NW China. *Geol. J.* **2020**, *55*, 7998–8016. [CrossRef]

44. Wang, X.T.; Fu, C.M.; Li, H.S. Basin-mountain coupling characters of northern edge of Qaidam Basin and the prospect area for sandstone-host U deposit. *Miner. Resour. Geol.* **2008**, *22*, 492–495, (In Chinese with English Abstract).

45. Liu, W.J.; Dang, H.L.; Huang, G.N.; Huang, X.H.; Liu, B.Q.; Zhang, Y.A.; Wang, W.C.; Qi, L.J. Metallogenic conditions and prospecting target of sand type uranium deposits in the Tuanyushan area of northern Qaidam Basin. *Northwestern Geol.* **2019**, *52*, 232–240, (In Chinese with English Abstract).

46. Liu, Y.; Yang, S.; Yin, Y.P.; Wang, J.L.; Hao, G.Q. Hydrocarbon fluid feature of the Shangyoushashan Formation sandstone in the northwest Qaidam Basin and its relationship to uranium mineralization. *J. East China Univ. Technol. Nat. Sci.* **2020**, *43*, 430–436, (In Chinese with English Abstract).

47. Qiao, J.X.; Zhao, X.G.; Liu, L.; Chen, Q. The relationship analysis of thrust structure and sandstone type uranium deposits at northern margin of Qaidam Basin. *J. East China Univ. Technol. Nat. Sci.* **2010**, *33*, 252–256, (In Chinese with English Abstract).

48. Lian, K.; Zhao, X.Q.; Wang, J.B.; Song, Y. Condition and Potential of Sandstone-type Uranium Metallization in Yuqia Area, Northern Qaidam Basin. *Uranium Geol.* **2020**, *36*, 145–155, (In Chinese with English Abstract).

49. Heath, J.E.; Dewers, T.A.; Mcpherson, B.; Nemer, M.B.; Kotula, P.G. Pore-lining phases and capillary breakthrough pressure of mudstone caprocks: Sealing efficiency of geologic CO_2 storage sites. *Int. J. Greenh. Gas Control.* **2012**, *11*, 204–220. [CrossRef]

50. Shi, H.C.; Jiang, C.X.; Sun, M.J.; Liao, Z.B.; Cheng, G.X.; Qi, T.S. Sealing capability assessment of mudstone caprock in the Upper Paleozoic, South Ordos Basin. *Pet. Geol. Recovery Effic.* **2015**, *22*, 9–16, (In Chinese with English Abstract).

51. Zhao, C.Y.; Du, M.L.; Shao, L.Y.; Chen, J.P.; Cheng, K.M.; He, Z.H. Types of organic facies and source rock assessment of the coal-measure mudstone in the turpan-hami basin. *Acta Geol. Sin.* **2010**, *72*, 169–179.

52. Meng, Z.P.; Xian, X.M. Analysis of the mechanical property of mudstone/shale in paralic coal measures and its influence factors. *J. Coal Sci. Eng.* **2013**, *19*, 1–7. [CrossRef]

53. Wang, Z.B. Current status and prospects of uranium geology developments of foreign in-situ leachable sandstone-type uranium deposits. *Uranium Geol.* **2002**, *18*, 9–20, (In Chinese with English Abstract).

54. Jin, R.S.; Feng, X.X.; Teng, X.M.; Nie, F.J.; Cao, H.Y.; Hou, H.Q.; Liu, H.X.; Miao, P.S.; Zhao, H.L.; Chen, L.L.; et al. Genesis of green sandstone/mudstone from middle Jurassic Zhiluo Formation in the Dongsheng Uranium Orefield, Ordos Basin and its enlightenment for uranium mineralization. *China Geol.* **2020**, *1*, 54–68. [CrossRef]

55. Jin, R.S.; Teng, X.M.; Li, X.G.; Si, Q.H.; Wang, W. Genesis of sandstone-type uranium deposits along the northern margin of the Ordos Basin, China. *Geosci. Front.* **2020**, *11*, 215–227. [CrossRef]

56. Spirakis, C.S. The roles of organic matter in the formation of uranium deposits in sedimentary rocks. *Ore Geol. Rev.* **1996**, *11*, 53–69. [CrossRef]

57. Jin, R.S.; Cheng, Y.H.; Li, J.G.; Sima, X.Z.; Miao, P.S.; Wang, S.Y.; Ao, C.; Li, H.L.; Li, Y.F.; Zhang, T.F. Late Mesozoic continental basin "Red and Black beds" coupling formation constraints on the sandstone uranium mineralization in northern China. *Geol. China* **2017**, *44*, 205–223, (In Chinese with English Abstract).

58. Jin, R.S.; Yu, R.A.; Yang, J.; Zhou, X.X.; Teng, X.M.; Wang, S.B.; Si, Q.H.; Zhu, Q.; Zhang, T.F. Paleo-environmental constraints on uranium mineralization in the Ordos Basin: Evidence from the color zoning of U-bearing rock series. *Ore Geol. Rev.* **2019**, *104*, 175–189. [CrossRef]

59. Liu, Z.Y.; Peng, S.P.; Qin, M.K.; Liu, H.X.; Geng, Y.Y.; Zhang, X.; Ding, B.; Xiu, X.Q. Origin and Role of Kaolinization in Roll-Front Uranium Deposits and Its Response to Ore-Forming Fluids in the Yili Basin, China. *Geofluids* **2018**, *2018*, 7847419. [CrossRef]

60. Zhao, L.; Cai, C.F.; Jin, R.S.; Li, J.G.; Li, H.L.; Wei, J.L.; Guo, H.; Zhang, B. Mineralogical and geochemical evidence for biogenic and petroleum-related uranium mineralization in the Qianjiadian deposit, NE China. *Ore Geol. Rev.* **2018**, *101*, 273–292. [CrossRef]

61. Jiang, X.Y. Discussion on the metallogenic conditions of exogenous uranium deposits: Paleoclimatic conditions. *Radiogeology* **1983**, *2*, 9–13. (In Chinese)

62. Chen, D.S.; Liu, W.S.; Jia, L.C. Paleo-climate evolution in China and its contrl on the metallization of sandstone type uranium deposit of Meso-Cenozoic basins. *Uranium Geol.* **2011**, *27*, 321–326+344, (In Chinese with English Abstract).

63. Cheng, Y.H.; Wang, S.Y.; Jin, R.S.; Li, J.G.; Ao, C.; Teng, X.M. Global Miocene tectonics and regional sandstone-style uranium mineralization. *Ore Geol. Rev.* **2019**, *106*, 238–250. [CrossRef]

64. Wu, Z.J.; Han, X.Z.; Lin, Z.X.; Li, Z.N.; Ji, H.; Yin, D.F.; Jiang, Z.; Hu, H. Tectonic, sedimentary, and climate evolution of meso-cenozoic basins in North China and its significance of coal accumulation and uranium mineralization. *Geotecton. Metallog.* **2020**, *44*, 710–724, (In Chinese with English Abstract).

65. Chen, Z.L.; Chen, X.H.; Wang, X.F.; Cheng, H.H. Characteristics of in-situ leachable sandstone-type uranium deposit and preliminary study on ore-forming conditions. *Miner. Depos.* **2002**, *21*, 853–856, (In Chinese with English Abstract).

66. Chen, D.S.; Li, S.X.; Cai, Y.Q. A discussion on research situation and development direction of sandstone-type uranium deposits in the Meso-Cenozoic basin of China. *Acta Sedimentol. Sin.* **2003**, *21*, 113–117, (In Chinese with English Abstract).

67. Jiao, Y.Q.; Wu, L.Q.; Peng, Y.B.; Rong, H.; Ji, D.M.; Miao, A.S.; Li, H.L. Sedimentary tectonic setting of the deposition-type uranium deposits forming in the Paleo-Asian tectonic domain, North China. *Earth Sci. Front.* **2015**, *22*, 189–205, (In Chinese with English Abstract).

68. Zhao, J.F.; Zeng, X.; Tian, J.X.; Hu, C.; Wang, D.; Yan, Z.D.; Wang, K.; Zhao, X.D. Provenance and paleogeography of the Jurassic Northwestern Qaidam Basin (NW China): Evidence from sedimentary records and detrital zircon geochronology. *J. Asian Earth Sci.* **2020**, *190*, 104060. [CrossRef]

69. Li, L.L.; Guo, Z.J.; Guan, S.W.; Zhou, S.P.; Wang, M.Z.; Fang, Y.N.; Zhang, C.C. Heavy mineral assemblage characteristics and the Cenozoic paleogeographic evolution in southwestern Qaidam Basin. *Sci. China Earth Sci.* **2015**, *58*, 859–875, (In Chinese with English Abstract). [CrossRef]

70. Shen, A.J.; Zhu, G.H.; Shou, J.F.; Xu, Y. A research on E_3^1-N_1-N_2^1 clastic rock reservoir in Yuejin Area, Qaidam Basin, Northwest China. *Acta Sediment. Sin.* **2001**, *19*, 71–78, (In Chinese with English Abstract).

71. Guan, P.; Jian, X. The Cenozoic sedimentary record in Qaidam Basin and its implication for tectonic evolution of the northern Tibetan Plateau. *Acta Sedimentol. Sin.* **2013**, *31*, 824–833, (In Chinese with English Abstract).

72. Wang, Y.Q.; Liu, Y.T.; Huang, G.P.; Li, S.M.; Xia, Z.Y.; Gong, Q.S.; Liu, Z.G.; Song, G.Y.; Zhu, C. *Paleogene–Neogene Sedimentary System and Oil-Gas Distribution in Western Qaidam Basin*; Petroleum Industry Press: Beijing, China, 2014; pp. 1–7. (In Chinese)

73. Xiao, P.; Tang, C.; Wei, J.L.; Xu, Z.L.; Zeng, H.; Liu, H.J. Sedimentary facies of the Sifangtai Formation in the southern Daqing placanticline and its controls to uranium mineralization. *Geol. Surv. Res.* **2018**, *41*, 18–23, (In Chinese with English Abstract).

74. Xu, Z.L.; Tang, C.; Li, J.G.; Wei, J.L.; Zeng, H.; Xiao, P.; Liu, H.J.; Chen, L.L. Sequence stratigraphy of the Sifangtai Formation and its relationship with uranium mineralization in the Sanzhao depression, northern Songliao basin. *Geol. Surv. Res.* **2018**, *41*, 24–31, (In Chinese with English Abstract).

75. Hu, F.; Li, J.G.; Liu, Z.J.; Zhao, D.M.; Wan, T.; Xu, C. Sequence and sedimentary characteristics of upper Cretaceous Sifangtai Formation in northern Songliao Baisn, northeast China: Implications for sandstone-type uranium mineralization. *Ore Geol. Rev.* **2019**, *111*, 102927. [CrossRef]
76. Cheng, X.Y.; Zhang, T.F.; Cheng, Y.H.; Wang, S.Y.; Tian, J. Paleosedimentary environment evolution of Zhiluo Formation in Tarangaole area, northern margin of the Ordos Basin-evidence from geochemical characteristics. *North China Geol.* **2021**, *44*, 1–3. (In Chinese)
77. Abudukeyumu, A.; Song, H.; Chi, G.X.; Li, Q.; Zhang, C.J. Quaternary uranium mineralization in the Qaidam Basin, northern Tibetan Plateau: Insights from petrographic and C-O isotopic evidences. *Ore Geol. Rev.* **2022**, *140*, 104628. [CrossRef]
78. Taylor, S.R.; McLennan, S.M. *The Continental Crust: Its Composition and Evolution GeoSci. Texts*; Blackwell Scientific Publications: Oxford, UK, 1985; p. 312.
79. Singh, P.; Rajamani, V. Geochemistry of the floodplain sediment of the Kaveri River, southern India. *J. Sediment. Res.* **2001**, *71*, 50–60. [CrossRef]
80. Nesbitt, H.W.; Young, G.M. Early Proterozoic climates and plate motions inferred from major element chemistry of lutites. *Nature* **1982**, *299*, 715–717. [CrossRef]
81. Andersson, P.O.D.; Worden, R.H. Mudstones of the Tanqua Basin, South Africa: An analysis of lateral and stratigraphic variations within mudstones, and a comparison of mudstones within and between turbidite fans. *Sedimentology* **2004**, *51*, 479–502. [CrossRef]
82. Fedo, C.M.; Nesbitt, H.W.; Young, G.M. Unraveling the effects of potassium metasomatism in sedimentary rocks and paleosols, with implications for paleoweathering conditions and provenance. *Geology* **1995**, *23*, 921–924. [CrossRef]
83. Fedo, C.M.; Eriksson, K.A.; Krogstad, E.J. Geochemistry of shales from the Archean (3.0 Ga) Buhwa Greenstone Belt, Zimbabwe: Implications for provenance and source-area weathering. *Geochim. Cosmochim. Acta* **1996**, *60*, 1751–1763. [CrossRef]
84. Roddaz, M.; Viers, J.; Brusset, S.; Baby, P.; Boucayrand, C.; Herail, G. Controls on weathering and provenance in the Amazonian foreland basin: Insights from major and trace element geochemistry of Neogene Amazonian sediments. *Chem. Geol.* **2006**, *226*, 31–65. [CrossRef]
85. Schoenborn, W.A.; Fedo, C.M. Provenance and paleoweathering reconstruction of the Neoproterozoic Johnnie Formation, southeastern California. *Chem. Geol.* **2011**, *285*, 231–255. [CrossRef]
86. Mclennan, S.M. Weathering and global denudation. *J. Geol.* **1993**, *101*, 295–303. [CrossRef]
87. Nesbitt, H.W.; Young, G.M. Prediction of some weathering trends of plutonic and volcanic rocks based on thermodynamic and kinetic considerations. *J. Geol.* **1984**, *48*, 1523–1534. [CrossRef]
88. Visser, J.N.J.; Young, G.M. Major element geochemistry and paleoclimatology of the Permo-Carboniferous glacigene Dwyka Formation and post-glacial mudrocks in southern Africa. *Palaeogeogr. Palaeoclimatol. Palaeoecol.* **1990**, *81*, 49–57. [CrossRef]
89. Song, B.; Yan, Q.R.; Xiang, Z.J.; Chen, H.M.; Li, J.L. Petrography and geochemistry of clastic rocks and their constraints on the tectonic setting of the Middle Triassic Pingxiang basin, Southern Part of Guangxi. *Geol. Bull. China* **2014**, *33*, 2032–2050, (In Chinese with English Abstract).
90. Hou, M.C.; Jiang, W.J.; Ni, S.J.; Huang, H.; Luo, W.; Shi, X.; Miu, Z.L. Geochemical characteristic of the lower and middle jurassic clastic rocks in the southern margin of the Yili Basin, Xinjiang and its Constraints on Provenance. *Acta Geol. Sin.* **2016**, *90*, 3337–3351, (In Chinese with English Abstract).
91. Floyd, P.A.; Leveridge, B.E. Tectonic environment of the Devonian Gramscatho basin, south Cornwall: Framework mode and geochemical evidence from turbiditic sandstones. *J. Geol. Soc.* **1987**, *144*, 531–542. [CrossRef]
92. McLennan, S.M.; Hemming, S.R.; McDaniel, D.K. Geochemical approaches to sedimentation, provenance and tectonics. In *Processes Controlling the Composition of Clastic Sediments*; Johnsson, M.J., Basu, A., Eds.; Geological Society of America: Boulder, CO, USA, 1993; Volume 284, pp. 21–40.
93. Mclennan, S.M. Relationships between the trace element composition of sedimentary rocks and upper continental crust. *Geochem. Geophys. Geosyst.* **2001**, *2*, 1021–1024. [CrossRef]
94. Zhang, T.F.; Sun, L.X.; Zhang, Y.; Cheng, Y.H.; Li, Y.F.; Ma, H.L.; Lu, C.; Yang, C.; Guo, G.W. Geochemical characteristics of the Jurassic Yan'an and Zhiluo Formations in the northern margin of Ordos Basin and their Paleoenvironmental implications. *Acta Geol. Sin.* **2016**, *90*, 3454–3472, (In Chinese with English Abstract).
95. Yu, D.D.; Zhang, Y.S.; Xing, E.Y.; Zuo, Z.F.; Hou, X.H.; Wang, L.L.; Zhao, W.Y. Petrological characteristics and sedimentary environment of the surface mixed rocks in nanyishan structure, Western Qaidam Basin. *Acta Geol. Sin.* **2018**, *92*, 2068–2080, (In Chinese with English Abstract).
96. Russell, A.D.; Morford, J.L. The behavior of redox-sensitive metals across a laminated–massive–laminated transition in Saanich Inlet, British Columbia. *Mar. Geol.* **2001**, *174*, 341–354. [CrossRef]
97. Tribovillard, N.; Algeo, T.J.; Lyons, T.; Riboulleau, A. Trace metals as paleoredox and paleoproductivity proxies: An update. *Chem. Geol.* **2006**, *232*, 12–32. [CrossRef]
98. Chang, H.J.; Chu, X.L.; Feng, L.J.; Huang, J.; Zhang, Q.R. Redox sensitive trace elements as paleoenvironments proxies. *Geol. Rev.* **2009**, *55*, 731–739, (In Chinese with English Abstract).
99. Broecker, W.S.; Peng, T.H. *Tracers in the Sea*; Eldigio Press; Columbia University: Palisades, NY, USA, 1982; 689p.
100. Anderson, R.F.; Fleisher, M.Q.; LeHuray, A.P. Concentration, oxidation state and particulate flux of uranium in the Black Sea. *Geochim. Cosmochim. Acta* **1989**, *53*, 2215–2224. [CrossRef]

101. Calvert, S.E.; Pedersen, T.F. Geochemistry of recent oxic and anoxic sediments: Implications for the geological record. *Mar. Geol.* **1993**, *113*, 67–88. [CrossRef]
102. Hastings, D.W.; Emerson, S.R.; Mix, A.C. Vanadium in foraminiferal calcite as a tracer for changes in the areal extent of reducing sediments. *Paleoceanography* **1996**, *11*, 665–678. [CrossRef]
103. Achterberg, E.P.; Van den Berg, C.M.G.; Colombo, C. High resolution monitoring of dissolved Cu and Co in coastal surface waters of the western North Sea. *Contin. Shelf Res.* **2003**, *23*, 611–623. [CrossRef]
104. Jones, B.; Manning, D. Comparison of geochemical indices used for the interpretation of palaeoredox conditions in ancient mudstones. *Chem. Geol.* **1994**, *111*, 111–129. [CrossRef]
105. Lermanm, A. *Lakes: Chemistry, Geology, Physics*; Springer: Berlin/Heidelberg, Germany, 1978; pp. 79–83.
106. Cheng, F.; Guo, Z.J.; Jenkins, H.S.; Fu, S.T.; Cheng, X. Initial rupture and displacement on the Altyn Tagh fault, northern Tibetan Plateau: Constraints based on residual Mesozoic to Cenozoic strata in the western Qaidam Basin. *Geosphere* **2015**, *11*, 921–942. [CrossRef]
107. Bao, J.; Wang, Y.D.; Song, C.H.; Feng, Y.; Hu, C.H.; Zhong, S.R.; Yang, J.W. Cenozoic sediment flux in the Qaidam Basin, northern Tibetan Plateau, and implications with regional tectonics and climate. *Glob. Planet. Chang.* **2017**, *155*, 56–69. [CrossRef]
108. Jin, R.S.; Miao, P.S.; Sima, X.Z.; Li, J.G.; Zhao, H.L.; Zhao, F.Q.; Fen, X.X.; Chen, Y.; Chen, L.L.; Zhao, L.J.; et al. Structure styles of mesozoic-cenozoic U-bearing rock series in Northern China. *Acta Geol. Sin.* **2016**, *90*, 2104–2116. [CrossRef]
109. Li, J.G.; Zhang, B.; Jin, R.S.; Si, Q.H.; Miao, P.S.; Li, H.L.; Cao, M.Q.; Wei, J.L.; Chen, Y. Uranium mineralization of coupled supergene oxygen-uranium bearing fluids and deep acidic hydrocarbon bearing fluids in the Qianjiadian Uranium Deposit, Kailu Basin. *Geotecton. Metallog.* **2020**, *44*, 576–589, (In Chinese with English Abstract).